Strategy to overcome recombination limited photocurrent generation in CsPbX 3 nanocrystal arrays

Wasim J Mir, Clément Livache, Nicolas Goubet, Bertille J Martinez, Amardeep Jagtap, Audrey Chu, Nathan Coutard, Hervé Cruguel, Thierry Barisien, Sandrine Ithurria, et al.

Strategy to overcome recombination limited photocurrent generation in $CsPbX_3$ nanocrystal arrays

Wasim J. Mir[1,2,$], Clément Livache[1,3,$], Nicolas Goubet[1,3], Bertille Martinez[1,3], Amardeep Jagtap[1], Audrey Chu[1,3], Nathan Coutard[4], Hervé Cruguel[1], Thierry Barisien[1], Sandrine Ithurria[3], Angshuman Nag[2], Benoit Dubertret[3], Abdelkarim Ouerghi[5], Mathieu G. Silly[6], Emmanuel Lhuillier[1*]

[1]Sorbonne Universités, UPMC Univ. Paris 06, CNRS-UMR 7588, Institut des NanoSciences de Paris, 4 place Jussieu, 75005 Paris, France.
[2]Department of Chemistry, Indian Institute of Science Education and Research (IISER), Pune 411008, India.
[3]Laboratoire de Physique et d'Étude des Matériaux, ESPCI-ParisTech, PSL Research University, Sorbonne Universités UPMC Univ Paris 06, CNRS, 10 rue Vauquelin 75005 Paris, France.

[4]Laboratoire de Chimie et Biologie des Métaux ; Université Grenoble Alpes, CNRS, CEA; 17 rue des Martyrs, 38000 Grenoble, France.

[5]Centre de Nanosciences et de Nanotechnologies, CNRS, University of Paris-Sud, Université Paris-Saclay, C2N, Marcoussis 91460, France.
[6]Synchrotron-SOLEIL, Saint-Aubin, BP48, F91192 Gif sur Yvette Cedex, France.

Abstract: We discuss the transport properties of $CsPbBr_xI_{3-x}$ perovskite nanocrystal arrays as a model ensemble system of caesium lead halide-based perovskite nanocrystal arrays. While this material is very promising for the design of light emitting diodes, laser and solar cells, very little work has been devoted to the basic understanding of their (photo)conductive properties in an ensemble system. By combining DC and time-resolved photocurrent measurements, we demonstrate fast photodetection with time response below 2 ns. The photocurrent generation in perovskite nanocrystal-based arrays is limited by fast bimolecular recombination of the material, which limits the lifetime of the photogenerated electron-hole pairs. We propose to use nanotrench electrodes as a strategy to ensure that the device size fits within the obtained diffusion length of the material in order to boost the transport efficiency and thus observed an enhancement of the photoresponse by a factor of 1,000.

Keywords: $CsPbX_3$, Perovskite nanocrystals, Transport, Photoconduction, Electronic Properties

$ these two authors have equal contributions

To whom correspondence should be sent: el@insp.upmc.fr

Lead halide-based perovskite materials have raised significant scientific and technological interests in the field of solar cells because of their defect-tolerant band structure.[1] This structure leads to large open-circuit voltages (>1 V) and thus to high power conversion efficiencies.[2] Improved efficiencies of around 20 % for hybrid perovskites[3] and above 13% for perovskite quantum dot-based devices[4],[5] have been reported so far. The idea of using these defect-tolerant lead halide-based perovskite nanocrystals for designing high-efficiency light-emitting devices was later proposed by the Kovalenko group.[6] A paradigm shift was proposed: instead of preventing the wave function from encountering surface traps by building a shell around the nanocrystal, a defect-tolerant material ensures that no surface traps are generated in the mid-gap region. As a result, $CsPbX_3$ (with X a halide anion) nanocrystals are able to generate high photoluminescence (PL) efficiency6 (≈ 90 % based on core only objects) and are obtained through straightforward and reliable synthesis. Their exceptional light emitting properties have been used to demonstrate low thresholds for lasing,[7] single photon emission[8,9] and light-emitting diodes with narrow emission linewidth.[10,11,12,] As a result, both high light-emitting efficiency and defect-tolerant nature make them promising candidates for a new generation of nanocrystal-based optoelectronic devices.[13,14]

As a new class of colloidal nanomaterials, lead halide-based perovskite nanocrystals (PNCs) raise strong interest because of their unique properties, yet reveal some new challenges. In particular, these materials present some stability issues: PNCs degrade under an electron beam[15] and undergo structural phase changes or ligand-induced stoichiometry change.[16] As a result, PNCs need to be handled with great care and the conventional method to build conductive nanocrystal-based films need to be revised. For example, a phase transfer ligand exchange toward S^{2-} capping, although quite successful for metal chalcogenide nanocrystals,[17,18] cannot be applied to PNCs. Indeed, such a ligand exchange performed on PNCs leads to the formation of a conductive and photoresponsive film of…PbS nanocrystals (see Supporting Information (SI) and Figure S6). Similarly, ion gel gating[19,20] cannot be straight forwardly applied because the ion gel dissolves the PNCs. As a consequence, the whole surface chemistry toolbox used to tune the tunnel barrier associated with the capping ligands and used to make film photoconductive needs to be revisited.

The recent report of PNC-based solar cell4 with relatively high photon conversion efficiency (13 %) has demanded for a deeper investigation of the charge transport properties of PNC arrays. However current transport experiments[21,22,23] from PNC-based devices have been performed on diode structures. [24,25] In such device geometries, the transport of the PNC layer is blurred with effects coming from the electron and hole extraction layers. This makes the basic understanding of the transport more complex.

In this paper, we use a combination of optical and photoemission spectroscopy and transport measurements to highlight the current limitations of the photocurrent generation in PNC arrays. We provide evidence that the fast bimolecular recombination of PNC is the main limitation and is responsible for the short photocarrier lifetime. We thus propose to use a nanotrench device geometry to boost the carrier injection at a given high field and enhance photocurrent generation by a factor of 1,000.

We conducted transport measurements on a series of $CsPbBr_xI_{3-x}$ samples. This manuscript will focus on one particular PNC composition $CsPb(Br_{0.65},I_{0.35})_3$. Energy dispersive X-ray spectroscopy (see Figure S1) reveals that the actual composition is slightly more Br-rich than expected and that the actual iodine content is close to 25%. The choice of $CsPb(Br_{0.65},I_{0.35})_3$ was initially driven by a trade-off between the material stability (higher for Br-rich samples) and the optimal value of the band gap for solar cell application (better suited with iodine).

These $CsPb(Br_{0.65},I_{0.35})_3$ PNCs were grown using previously described methods[5,7] and present a band edge energy of 2.29 eV (see Figure 1(a)), which is close to the bulk band gap of the material having same halide composition and also consistent with their weak confinement. Transmission electron microscopy (TEM) imaging (see Figure 1(b)) indeed reveals a particle size in the range of 12 ± 2 nm, which is larger than the Bohr diameter of this material (7 nm).6 Their time-resolved PL decay dynamics (see Figure 1(c)) is fitted with a biexponential decay function with two time constants, 5 ns and 25 ns, which will be further discussed in the results and discussion section. This study of the spectroscopic properties of $CsPb(Br_{0.65},I_{0.35})_3$ PNCs is complemented by X-ray photoemission spectroscopy, intended to probe the electronic spectrum on the absolute energy scale.[26] This work is of utmost importance to probe and quantify the Schottky barrier at the metal-PNC interface. Measurements were conducted at the TEMPO beamline of the SOLEIL synchrotron on PNC films prepared by following the same protocol used for transport studies at the device scale. For more details about the processing of the photoemission data as well as the analysis of the core level see Figure S2-S4 given in the SI. The cut-off of the secondary electrons reveals the work function (WF) to be ≈ 4.1 eV, see Figure S5(a) and is used to scale the spectrum on the absolute energy scale. The low binding energies part of the XPS spectrum, unveils the energy of the valence band with respect to the Fermi level (≈1.45 eV) (see Figure S5(b)). The PL band gap 2.29 eV (see Figure 1(a)) is used to set the energy of the conduction band with respect to the valence band. This allows us to propose the electronic energy spectrum for the $CsPb(Br_{0.65},I_{0.35})_3$ PNC ensemble (see Figure 1(d)). The Fermi level is quite deep in the band gap of the material but lies closer to the conduction band, suggesting a slight *n*-type character of the PNCs, which is consistent with recent magneto-optical spectroscopic measurements.[27]

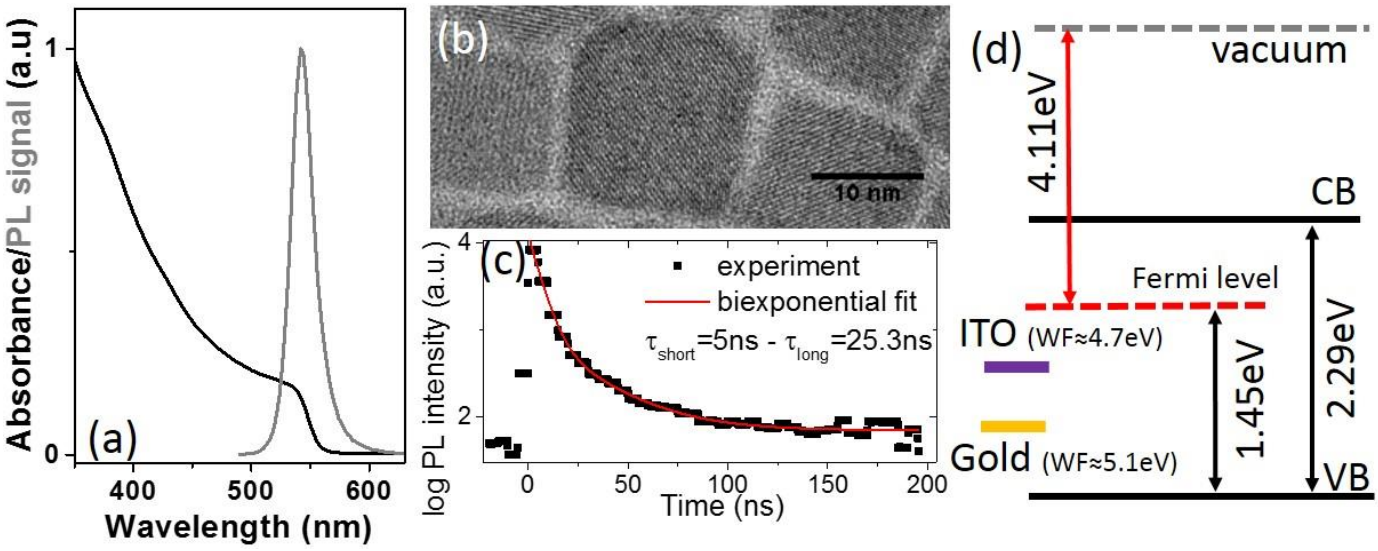

Figure 1. (a) Absorption and PL spectra of $CsPb(Br_{0.65},I_{0.35})_3$. (b) TEM image of the $CsPb(Br_{0.65},I_{0.35})_3$ PNCs. (c) Room temperature time-resolved PL signal for a film of $CsPb(Br_{0.65},I_{0.35})_3$ PNCs. Both photoemission and PL measurements were carried out on thin films treated with saturated lead acetate in methylacetate. (d) Electronic structure in absolute energy scale of $CsPb(Br_{0.65},I_{0.35})_3$ PNCs. The WF of gold (5.1 eV) and ITO (4.7 eV) are also provided.

After synthesis of the desired PNC composition, colloidal dispersion of PNCs was drop-casted over predesigned electrodes (see the methods section for details about fabrication and see the inset of Figure 2(b) for the schematic of the device used). The insulating long chain oleylammonium capping ligands were then removed by following a previously reported procedure.4 Briefly, thin film of the PNCs is dipped in a solution of lead acetate in methyl acetate. Using Fourier-transform infrared spectroscopy (FTIR), we find that the absorption relative to the C-H bond, which is signature of long chain organic capping ligands, is strongly suppressed after the ligand exchange step (see Figure S7(a)).

Finally, the device was mildly annealed at 100 °C for two minutes to dry the film and improve the inter-nanocrystal coupling. A higher annealing temperature (200 °C) or longer annealing time leads to strong inter-PNC sintering, resulting in a loss of their nano-crystalline aspect as revealed by scanning electron microscopy (SEM) imaging Figure S7(d)-S7(g), X-ray diffraction Figure S7(b) and conduction measurements Figure S8(a)-S8(b). On the other hand, ligand exchange followed by a short mild annealing at 100 °C preserves the PNC aspect, and only a limited change, from 10 to 15 nm, of the Scherrer size extracted from the diffraction pattern is observed (see Figure S7(c)).

Thin films of PNCs reaching a thickness of 200-400 nm were prepared using a multistep procedure in order to obtain an efficient ligand exchanged film. Multistep deposition is also used to fill up the pin holes or cracks generated by the volume reduction resulting from the removal of long chain organic ligands and annealing steps**.** Once deposited on metallic electrodes, the thin film of $CsPb(Br_{0.65},I_{0.35})_3$ PNCs presents a conductive ohmic behavior (see Figure 2(a)), in spite of the somewhat large band offset (≈ 0.5 eV for holes) between the bands of $CsPb(Br_{0.65},I_{0.35})_3$ and the gold electrodes (see Figure 1(d)). Under 532 nm irradiation (2 $W.cm^{-2}$), a significant rise in the conductance is observed, typically by four orders of magnitude (see Figure 2(a)). We further cross-checked that the method used to make the thin film conductive and photoconductive is not limited to this particular halide content. In particular, we demonstrated that the method can be applied to other shapes, including nanocubes (0D objects) and nanoplatelets[28] (2D objects, NPL) (see Figure S9), and to other Br:I ratios (see Figure S10). The typical responsivity of the film spans from 200 $\mu A.W^{-1}$ to 1 $mA.W^{-1}$ depending on the incident power. The scaling of the photocurrent with the incident light power follows a power law with a 0.64 exponent[29] (see Figure 2(b)). This value is closer to 0.5 expected for bimolecular recombination (electron-hole recombination through radiative and non-radiative paths) than to the value of 1 that results from a monomolecular process (trapping) usually observed for metal chalcogenide nanocrystals.[30] This supports the hypothesis of the lower role of surface trapping in PNCs, as expected for a defect-tolerant material in which trap states are away from the band gap. We also investigated the temperature dependence of the current (see Figure 2(c)). Close to room temperature, the current follows an Arrhenius law, which suggests that transport occurs through a hopping process to the nearest neighbour. The associated activation energy (240 meV) is smaller than half the band gap expected for an intrinsic semiconductor and is qualitatively consistent with the deviation of the Fermi level with respect to the middle of the band gap observed from X-ray photoemission and PL spectroscopy (see Figure 1(d)).

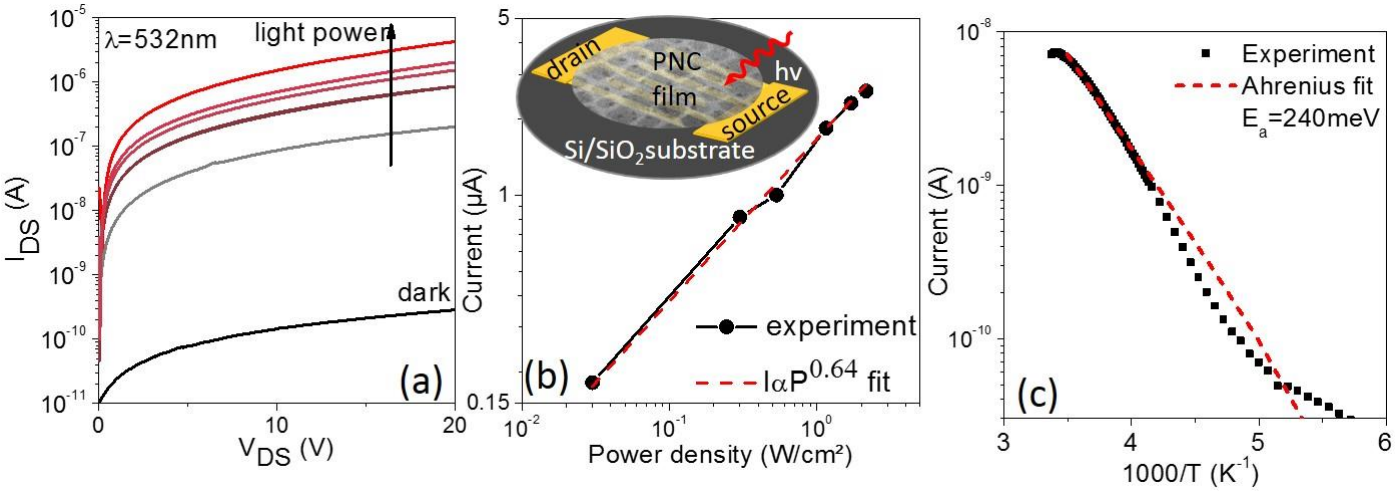

Figure 2. (a) IV curves of a film of $CsPb(Br_{0.65},I_{0.35})_3$ PNCs under dark conditions and under illumination at different light irradiance (λ=532 nm), under ambient atmosphere and at room temperature over 20 µm spaced interdigitated Au electrodes. (b) Current as a function of the light irradiance (λ=532 nm) for the same film shown in part (a). The inset shows scheme of the device. (c) Current under a voltage of 20 V as a function of temperature for a film of $CsPb(Br_{0.65},I_{0.35})_3$ PNCs measured under vacuum and in dark conditions.

We then investigated time-resolved carrier dynamics at the device scale. This is especially challenging because of the insulating character of the film. Under dark conditions, film resistance is typically in the 10 GΩ range and this is a crucial

difference with respect to narrower band gap nanocrystals (PbSe) previously probed using a high bandwidth transient photocurrent setup.[31,32] Measuring fast dynamics in the GHz range requires a special design where both sample stimulation (pulsed ns laser) and acquisition stage have to be compatible with the targeted GHz bandwidth of the setup (see Figure 3(a) for the schematic of the setup). The experiments are conducted on transparent electrodes made of ITO so as to (i) reduce the large Schottky barrier experienced by the electron, and (ii) to avoid any heating effects of the substrate which may lead to an artificial bolometric photoresponse of the device. We further cross-check that the phototransport properties of the films are effectively preserved (see Figure S11).

The transient photocurrent in PNCs is extremely fast with a main decay time of 1.2 ns. Typically, two time constants can be extracted from the decay curve (Figure 3(b) and S12): a fast component of ≈1.2 ns and a slower contribution around 7.3 ns. No long-lived tail is observed, which is consistent with a limited role of deep surface trap states, contrary to what can be observed on metal chalcogenide nanocrystals.[33] These transient photocurrent dynamics have to be correlated with the PL dynamics (Figure 1(c)). In such PL measurements, electron-hole pairs are generated by the laser pulse and the intra-PNC decay of the exciton population is followed. This PL decay is a good probe for the excited state carrier density. The fact that similar dynamics are observed using photocurrent experiments suggests that the current magnitude is actually driven by the photogenerated carrier population of PNCs.[31] This observation is also consistent with the flux dependence of the photocurrent Figure 2(b) which implies that the photocurrent generation is limited by interband gap recombination. In the current device, the diffusion length can be estimated using an Einstein diffusion equation: we found $L_D = \sqrt{D\tau} = \sqrt{\frac{\mu k_b T}{e}\tau} \approx 58 \ nm$, assuming a mobility of 0.26 $cm^2V^{-1}s^{-1}$ as recently determined from field effect transistor measurements[34] and τ = 5 ns from our photocurrent decay measurements. This is much smaller than the electrode spacing (20 µm). As a result, only the carriers in the closest vicinity of the electrodes can be collected as all the other carriers undergo recombination before reaching the electrodes. On the other hand, the obtained diffusion length value of ≈60 nm is very close to the length of a PNC layer used for solar cells (≈200 nm) which explain the recently obtained high power conversion efficiency.

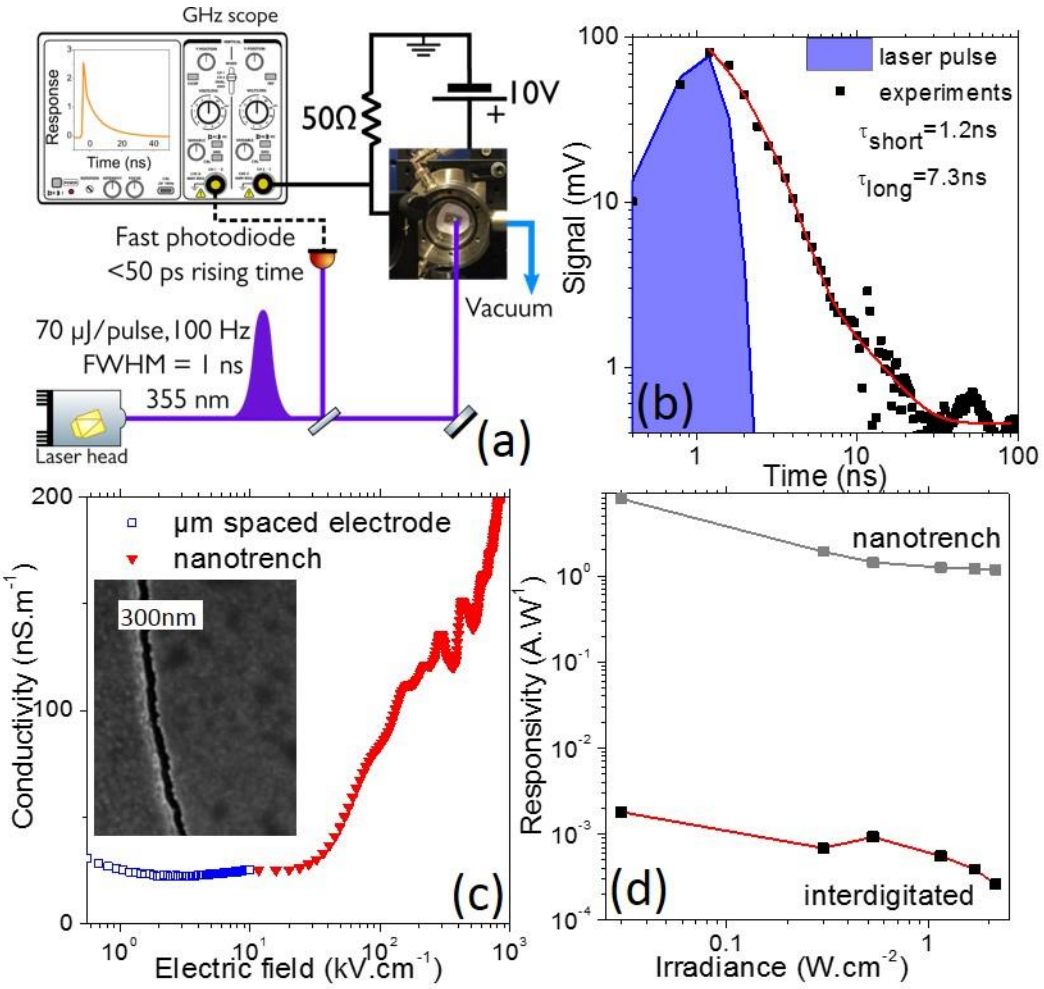

Figure 3. (a) Schematics of the high bandwidth transient photocurrent setup. (b) Transient photocurrent signal obtained in a film of $CsPb(Br_{0.65},I_{0.35})_3$ PNCs at room temperature. The film is deposited on interdigitated electrodes made of ITO/PET. (c) Conductivity as a function of the applied electric field under dark condition in the case of $CsPb(Br_{0.65},I_{0.35})_3$ PNCs. The data have been obtained from interdigitated electrodes at low electric field and from the nanotrench electrodes for the high field regime. The inset is a SEM image of uncovered nanotrench electrodes (i.e., the blackline is the trench). (d) Responsivity of a film of $CsPb(Br_{0.65},I_{0.35})_3$ PNCs over µm spaced interdigitated electrodes and over nanotrench electrodes.

We finally investigated the effect of electric field on transport, in particular in the high field regime. To do so, we built nanotrench electrodes see the inset of Figure 3(c). Along this nanotrench, the two electrodes lie 60 nm apart and have a high aspect ratio (length of 15 µm). Moreover, they present the key advantage of being built with a high fabrication success ratio (>80%) using only two optical lithography steps[30,35] in spite of the sub-wavelength size of the trench. To follow the electric field dependence of the conductance over almost four orders of magnitude, we used µm spaced interdigitated electrodes for the low field range and nanotrench electrodes for the high field range. The fact that the conductivity curves resulting from the two types of electrodes overlap (see Figure 3(c)) and suggests that the transport mechanism is unchanged. The latter remains dominated by the nearest neighbour hopping mechanism, which is consistent with the fact that 4-5 PNCs can fit within the nanotrench gap (60 nm). In the low field range, the conductance of the PNC film is field-independent. On the other hand, above 50 $kV.cm^{-1}$, we observe a significant rise in the conductance with the applied bias. This threshold corresponds to an energy drop per PNC of ≈50 meV, which likely results from the charging energy of the PNC. By applying a large electric field, we are able to inject charges in PNCs more efficiently and the effect of the electrode structure on photocurrent is quite dramatic. The responsivity of the film is enhanced by more than a factor 1,000 as we switch from µm spaced electrodes to nanoscale devices (see Figure 3(d)). This increase arises from a combination of (*i*) an easier charge injection into PNC and (*ii*) an increase of

gain due to the short inter-electrode spacing. In a photoconductor, the gain is the ratio of the photocarrier lifetime (≈ 5 ns) over the transit time (the time to go from one electrode to the other). In this nanotrench geometry, the transit time is reduced by a factor of 300 as compared to µm spaced electrodes.[30,36] Because of the n-type nature of these PNCs, the electron will recirculate several times during the hole carrier lifetime, leading to photogating[37] and to the observed enhanced photocurrent.[38]

In conclusion, using a combination of DC and time resolved transport measurements, we provide evidence that the photocurrent of PNC arrays is limited by the fast bimolecular recombination of the material. This leads to fast recombination of the photogenerated electron-hole pair which allows for high bandwidth photodetection with time response as short as 1.2 ns but limits the absolute photoresponse of the film. We then propose to use nanotrench electrodes to achieve better charge injection at high electric fields and maintained the best correlation between the device size and the material diffusion length. Thanks to this strategy, we have enhanced the photoresponse by a factor of 1,000.

"Supplementary Material" include informations about material synthesis, material characterization, photoemission data acquisition and processing, informations on film preparation for transport and additional transport measurements.

Acknowledgements

We acknowledge the use of clean room facilities from the consortium "Salles Blanches Paris Centre -SBPC". This work has been supported by the Region Ile-de-France in the framework of DIM Nano-K via the grant dopQD. This work was supported by French state funds managed by the ANR within the Investissements d'Avenir program under reference ANR-11-IDEX-0004-02, and more specifically within the framework of the Cluster of Excellence MATISSE. Wasim J. Mir acknowledges CEFIPRA for the Raman-Charpak fellowship and CSIR India for the PhD fellowship. EL is thankful for the support of the ERC starting grant (project: blackQD - grant 756225).

References

[1] H. Huang, M. I. Bodnarchuk, S. V. Kershaw, M. V. Kovalenko, and A. L. Rogach, ACS Energy Lett. **2**, 2071 (2017).
[2] F. Hao, C. C. Stoumpos, D. H. Cao, R. P. H. Chang, and M. G. Kanatzidis, Nat. Photon. **8**, 489 (2014).
[3] W. S. Yang, B. W. Park, E. H. Jung, N. J. Jeon, Y. C. Kim, D.U. Lee, S. S. Shin, J. Seo, E. K. Kim, J. H. Noh, S. I. Seok, Science **356**, 1376 (2017).
[4] A. Swarnkar, A. R. Marshall, E. M. Sanehira, B. D. Chernomordik, D. T. Moore, J. A. Christians, T. Chakrabarti, and J. M. Luther, Science **354**, 92 (2016).
[5] E. M. Sanehira, A. R. Marshall, J. A. Christians, S. P. Harvey, P. N. Ciesielski, L. M. Wheeler, P. Schulz, L. Y. Lin, M. C. Beard and Joseph M. Luther, Sci. Adv. **3,** eaao4204 (2017).
[6] L. Protesescu, S. Yakunin, M. I. Bodnarchuk, F. Krieg, R. Caputo, C. H. Hendon, R. X. Yang, A. Walsh, and M. V. Kovalenko, Nano Lett. **15**, 3692 (2015).
[7] S. Yakunin, L. Protesescu, F. Krieg, M. I. Bodnarchuk, G. Nedelcu, M. Humer, G. De Luca, M. Fiebig, W. Heiss, M. V. Kovalenko, Nat. Commun. **6**, 8056 (2015).
[8] Y. S. Park, S. Guo, N. S. Makarov, and V. I. Klimov, ACS Nano **9**, 10386 (2015).
[9] G. Rainò, G. Nedelcu, L. Protesescu, M. I. Bodnarchuk, M. V. Kovalenko, R. F. Mahrt, and T. Stöferle, ACS Nano **10**, 2485 (2016).

[10] J. Song, J. Li, X. Li, L. Xu, Y. Dong, and H. Zeng, Adv. Mater. **27**, 7162 (2015).
[11] E. Yassitepe, Z. Yang, O. Voznyy, Y. Kim, G. Walters, J. A. Castañeda, P. Kanjanaboos, M. Yuan, X. Gong, F. Fan, J. Pan, S. Hoogland, R. Comin, O. M. Bakr, L. A. Padilha, A. F. Nogueira, E. H. Sargent, Adv. Funct. Mater. **26**, 8757 (2016).
[12] Z. Xiao, R. A. Kerner, L. Zhao, N. L. Tran, K. M. Lee, T.-W. Koh, G. D. Scholes and B. P. Rand, Nat Phot. 11, 108 (2017).
[13] G. Konstantatos and E. H. Sargent, *Colloidal Quantum Dot Optoelectronics and Photovoltaics* (Cambridge University Press, Cambridge, 2013).
[14] D. V. Talapin, J. S. Lee, M. V. Kovalenko, and E. V. Shevchenko, Chem. Rev. **110**, 389 (2010).
[15] Z. Dang, J. Shamsi, F. Palazon, M. Imran, Q. A. Akkerman, S. Park, G. Bertoni, M. Prato, R. Brescia, L. Manna, ACS Nano **11**, 2124 (2017).
[16] Z. Liu, Y. Bekenstein, X. Ye, S. C. Nguyen, J. Swabeck, D. Zhang, S. T. Lee, P. Yang, W. Ma, A. P. Alivisatos, J. Am. Chem. Soc. **139**, 5309 (2017).
[17] A. Nag, M. V. Kovalenko, J. S. Lee, W. Liu, B. Spokoyny, and D. V. Talapin, J. Am. Chem. Soc. **133**, 10612 (2011).
[18] H. Wang, E. Lhuillier, Q. Yu, A. Mottaghizadeh, C. Ulysse, A. Zimmers, A. Descamps-Mandine, B. Dubertret, and H. Aubin, Phys. Rev. B **92**, 041403 (2015).
[19] E. Lhuillier, S. Ithurria, A. Descamps-Mandine, T. Douillard, R. Castaing, X. Z. Xu, P. L. Taberna, P. Simon, H. Aubin, B. Dubertret, J. Phys. Chem. C **119**, 21795 (2015).
[20] E. Lhuillier, A. Robin, S. Ithurria, H. Aubin, and B. Dubertret, Nano Lett. **14**, 2715 (2014).
[21] D. H. Kwak, D. H. Lim, H. S. Ra, P. Ramasamy, and J. S. Lee, RSC Adv. **6**, 65252 (2016).
[22] F. Palazon, F. Di Stasio, S. Lauciello, R. Krahne, M. Prato, and L. Manna, J. Mater. Chem. C **4**, 9179 (2016).
[23] F. Palazon, S. Dogan, S. Marras, F. Locardi, I. Nelli, P. Rastogi, M. Ferretti, M. Prato, R. Krahne, L. Manna, J. Phys. Chem. C **121**, 11956 (2017).
[24] Q. A. Akkerman, M. Gandini, F. D. Stasio, P. Rastogi, F. Palazon, G. Bertoni, J. M. Ball, M. Prato, A. Petrozza, L. Manna, Nat. Energy **2**, 16194 (2016).
[25] J. H. Im, C. R. Lee, J. W. Lee, S. W. Park, and N. G. Park, Nanoscale **3**, 4088 (2011).
[26] V. K. Ravi, G. B. Markad, and A. Nag, ACS Energy Lett. **1**, 665 (2016).
[27] D. Canneson, E.V. Shornikova, D. R. Yakovlev, T. Rogge, A. A. Mitioglu, M. V. Ballottin, P. C. M. Christianen, E. Lhuillier, M. Bayer, L. Biadala, Nano Lett. **17**, 6177 (2017).
[28] Q. A. Akkerman, S. G. Motti, A. R. Srimath Kandada, E. Mosconi, V. D'Innocenzo, G. Bertoni, S. Marras, B. A. Kamino, L. Miranda, F. De Angelis, A. Petrozza, M. Prato, L. Manna, J. Am. Chem. Soc. **138**, 1010 (2016).
[29] L. J. Willis, J. A. Fairfield, T. Dadosh, M. D. Fischbein, and M. Drndic, Nano Lett. **9**, 4191 (2009).
[30] E. Lhuillier, J. F. Dayen, D. O. Thomas, A. Robin, B. Doudin, and B. Dubertret, Nano Lett. **15**, 1736 (2015).
[31] J. Gao, A. F. Fidler, and V. I. Klimov, Nat. Commun. **6**, 8185 (2015).
[32] A. F. Fidler, J. Gao, and V. I. Klimov, Nat. Phys. **13**, 604 (2017).
[33] B. Martinez, C. Livache, N. Goubet, A. Jagtap, H. Cruguel, A. Ouerghi, E. Lacaze, M. G. Silly, and E. Lhuillier, J. Phys. Chem. C **122,** 859 (2018).
[34] X. Hu, H. Zhou, Z. Jiang, X. Wang, S. Yuan, J. Lan, Y. Fu, X. Zhang, W. Zheng, X. Wang, X. Zhu, L. Liao, G. Xu, S. Jin, A. Pan, ACS Nano **11,** 9869 (2017).
[35] J. F. Dayen, V. Faramarzi, M. Pauly, N. T. Kemp, M. Barbero, B. P. Pichon, H. Majjad, S. Begin-Colin, and B. Doudin, Nanotechnology **21**, 335303 (2010).
[36] H. Wang, E. Lhuillier, Q. Yu, A. Zimmers, B. Dubertret, C. Ulysse, and H. Aubin, ACS Nano **11**, 1222 (2017).
[37] G. Konstantatos and E. H. Sargent, Appl. Phys. Lett. **91**, 173505 (2007).
[38] F. Prins, M. Buscema, J. S. Seldenthuis, S. Etaki, G. Buchs, M. Barkelid, V. Zwiller, Y. Gao, A. J. Houtepen, L. D. A. Siebbeles, H. S. J. van der Zant, Nano Lett. **12**, 5740 (2012).